

PCCP

Physical Chemistry Chemical Physics

Accepted Manuscript

This article can be cited before page numbers have been issued, to do this please use: T. Schwarze, M. Al Akrami, J. Heinrich, V. Hergl, E. Sperlich, A. Kelling, T. Sprenger, N. Jahn, T. Klamroth and N. Kulak, *Phys. Chem. Chem. Phys.*, 2025, DOI: 10.1039/D5CP03172A.



This is an Accepted Manuscript, which has been through the Royal Society of Chemistry peer review process and has been accepted for publication.

Accepted Manuscripts are published online shortly after acceptance, before technical editing, formatting and proof reading. Using this free service, authors can make their results available to the community, in citable form, before we publish the edited article. We will replace this Accepted Manuscript with the edited and formatted Advance Article as soon as it is available.

You can find more information about Accepted Manuscripts in the [Information for Authors](#).

Please note that technical editing may introduce minor changes to the text and/or graphics, which may alter content. The journal's standard [Terms & Conditions](#) and the [Ethical guidelines](#) still apply. In no event shall the Royal Society of Chemistry be held responsible for any errors or omissions in this Accepted Manuscript or any consequences arising from the use of any information it contains.

ARTICLE

A sodium ion-selective photosensitizer: Dibrominated F-BODIPY as a fluorescence imaging and therapeutic agent

Thomas Schwarze,^{*a} Mazen Al Akrami,^a Julian Heinrich,^a Vinja Hergl,^a Eric Sperlich,^a Alexandra Kelling,^a Tobias Sprenger,^{a,b} Nicolas Jahn,^a Tillmann Klamroth^a and Nora Kulak^{*a}Received 00th January 20xx,
Accepted 00th January 20xx

DOI: 10.1039/x0xx00000x

Herein, we report that the production of singlet oxygen ($^1\text{O}_2$) is exclusively regulated by sodium ions in aqueous solution by the use of a Na^+ -selective photosensitizer (PS), a 2,6-dibrominated F-BODIPY dye equipped with benzo-15-crown-5. The PS showed an enhanced fluorescence quantum yield (Φ_f) and an enhanced singlet oxygen quantum yield (Φ_Δ) in the presence of Na^+ . A detailed theoretical study uncovered the underlying photophysical pathways which are responsible for both functional characteristics of the PS, therapeutic and Na^+ imaging properties.

1 Introduction

Photodynamic therapy (PDT) is a non-invasive and very powerful method to kill cancer cells by singlet oxygen ($^1\text{O}_2$) generated through light and a photosensitizer (PS).^{1,2} Several PSs, mainly porphyrin derivatives are approved for the PDT treatment for different types of cancer such as skin, lung, bladder, and breast cancer.³ In malign breast cancer cells the pH value can be more acidic and the Na^+ level is up to five times higher than in benign cells (raising from around 20 mM to over 100 mM Na^+).⁴ A very powerful and non-invasive but costly technique to visualise Na^+ in the human body is based on magnetic resonance imaging (MRI) of ^{23}Na .⁵ A more cost-effective method to image Na^+ in vivo is the use of fluorescence spectroscopy.^{6,7} For a precise identification and targeted light irradiation of tumor tissue, a fluorescence imaging-guided PDT is very helpful.^{8,9} A further class of promising triplet PSs for PDT are based on boron-dipyrromethene (BODIPY) dyes,^{10–12} when for instance substituted in 2,6-position with heavy atoms such as iodine^{13,14,15} or bromine¹⁶. Two decades ago, the group of Akkaya et al. reported on 2,6-dibromo-substituted F-BODIPYs as triplet PSs to efficiently produce $^1\text{O}_2$.¹⁶ Further, O'Shea et al. published a while ago, that the $^1\text{O}_2$ generation rate can be regulated by protons.¹⁷ There, a photoinduced electron transfer (PET) is blocked by protonation of an amine donor.¹⁷ Moreover, in a pioneering work Akkaya et al. showed that a PS consisting of 2,6-diiodo- and 3,5-dipyridylethenyl-substituted F-BODIPY equipped in *meso*-position with a benzo-15-crown-5 can modulate and enhance $^1\text{O}_2$ production by both H^+ and Na^+ in

acetonitrile (ACN).¹⁸ Meanwhile, some factors that control the $^1\text{O}_2$ efficiency have been uncovered such as pH, light, hydrogen peroxide, nucleic acids, proteins etc.^{18–21}

In a recent study, we reported on a benzo-15-crown-5-equipped F-BODIPY dye **1a** (cf. Scheme 1) for a reliable fluorescence detection of Na^+ in the pH range from 3 to 10 by fluorescence enhancement caused by an off-switching of a PET by Na^+ in aqueous solution.²² Herein, we now report on a detailed experimental and theoretical study of the regulation of $^1\text{O}_2$ exclusively by Na^+ and the fluorescence sensing of Na^+ by a PS in ACN and aqueous solution. Our overriding goal is to design a PS which shows an enhanced $^1\text{O}_2$ production as well as an enhanced fluorescence response only in malign, but not in benign tissue. As a trigger we selected the enhanced Na^+ level in breast cancer cells. By fine tuning the Na^+ complexing abilities of the Na^+ -responsive PS (dissociation constant K_d) we aimed to manipulate the $^1\text{O}_2$ evolution and fluorescence response. We designed PS **1** to be both, a therapeutic and an imaging agent regulated by the enhanced Na^+ level in tumor tissue. PS **1** is a combination of the photostable triplet PS **2**,²³ a 2,6-dibromo-substituted F-BODIPY dye, and the pH-stable and Na^+ -selective binding unit **3**, benzo-15-crown-5²⁴ (Figure 1).

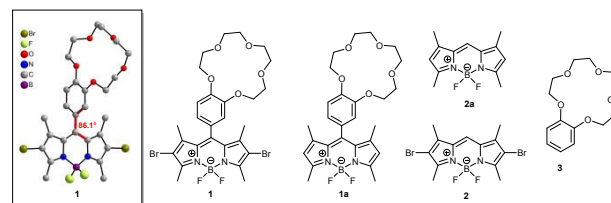


Figure 1 Studied Na^+ -selective 2,6-dibrominated F-BODIPY PS **1** (left: molecular structure obtained from XRD) and reference compounds **1a**, **2**, **2a** and **3**. H atoms are omitted for clarity.

2 Results and discussion

A bromination at positions 2 and 6 of the F-BODIPY **1a**²² core with *N*-bromosuccinimide (NBS) yielded the novel PS **1** in a moderate yield

^a Institute of Chemistry, University of Potsdam, 14476 Potsdam, Germany. E-mail: schwarzh@uni-potsdam.de, nora.kulak@uni-potsdam.de.

^b Faculty of Medicine, Health and Medical University (HMU), 14471 Potsdam, Germany.

[†]Supplementary Information available: Synthesis, data from NMR, EPR, UV/Vis and fluorescence spectroscopy, cyclic voltammetry, single crystal X-ray diffraction, DNA cleavage experiments and DFT calculations. See DOI: 10.1039/x0xx00000x



of 47%.²⁵ As a reference, the F-BODIPYs **PS 2** and **2a** without benzo-15-crown-5 moiety were synthesized as described.^{26,22} Benzo-15-crown-5 (**3**) is commercially available. The novel PS **1** was characterized by ¹H and ¹³C NMR spectroscopy as well as electrospray ionization mass spectrometry.²⁵ The molecular structure of **1** was confirmed by X-ray analysis (cf. Figure 1).²⁵ Single crystals of **1** were obtained by slow solvent evaporation (ethyl acetate/hexane, v/v, 1/1).

At first, we recorded UV/Vis absorption spectra of **1** and **2** in ACN (cf. Figure S2a). The absorption spectra of **1** and **2** are very similar, in the range from 350 nm to 550 nm, to each other. They show the most intense absorption band (S_0 to S_1 transition) with a local maximum (λ_{\max}) at about 525 nm (vibronic 0–0 state) with a shoulder at about 490 nm (vibronic 0–1 state).²⁷ The molar extinction coefficients (ϵ_{λ}) at λ_{\max} for **1** (77000 M⁻¹cm⁻¹) and **2** (75000 M⁻¹cm⁻¹) in ACN are comparable to each other, suggesting that the phenylic substituent in *meso*-position of the F-BODIPY in **1** does not significantly extend the π -electron system of the F-BODIPY chromophore. As found in the molecular structure of **1** the phenyl ring is almost orthogonal to the planar F-BODIPY core (dihedral angle 86.1°, cf. Figure 1) which electronically decouples the F-BODIPY from the benzo-15-crown-5. Then, we recorded UV/Vis absorption spectra of **1** and **2** ($c_{\text{dye}} = 10^{-5}$ M and 10^{-6} M, respectively) in different ACN/water mixtures and found a good solubility of **1** and **2** up to a ACN/water mixture of 1/9 (v/v) (cf. Figures S2c, S2d, S2e and S2f), but **2** showed a blue shift of λ_{\max} when the water amount was increased (cf. Figures 2d and 2f).²⁵ Thus, **2** is only an appropriate spectroscopic reference compound for **1** in ACN. Moreover, to ensure complete solubility of **1**, we decided for further investigation to use as an aqueous solution an ACN/water mixture of 1/3 (v/v). Further, the fluorescence emission maxima of **1** and **2** ($c = 10^{-6}$ M) were also very similar to each other in ACN (539 nm (**1**) and 540 nm (**2**)) (cf. Figure S6a), but their fluorescence quantum yields (Φ_f) differ from each other ($\Phi_f = 0.010$ (**1**), $\Phi_f = 0.207$ (**2**)).²⁵ The low Φ_f value of **2** is caused by a heavy atom quenching effect which is typical for a triplet PS.²⁸ Probably, in **1** an additional quenching process, such as in **1a** ($\Phi_f = 0.258^{22}$ in ACN(**1a**)), a reductive PET from the benzo-15-crown-5 (electron donor) to the excited and decoupled 2,6-dibrominated F-BODIPY core (electron acceptor) occurs.^{29–31} Solvent effects on the Φ_f values for **1** are found because the reductive PET in **1** is more favorable in polar solvents (cf. Table S3).²⁵ The low Φ_f values of **1**, **1a** and **2** in polar solvents make them suitable candidates as PS to produce efficiently ¹O₂ in ACN and aqueous solution. Then we monitored the ¹O₂ production by recording the absorbance of 1,3-diphenylisobenzofuran (DPBF) as a singlet oxygen scavenger at 410 nm in ACN, aqueous solution (ACN/water, v/v, 1/3) and 1,4-dioxane/dimethyl sulfoxide (v/v, 99/1).²⁵ The following singlet oxygen quantum yields (Φ_{Δ}) were calculated: 0.199 ± 0.010 for **1**, 0.239 ± 0.010 for **1a** and 0.495 ± 0.092 for **2** in ACN, 0.527 ± 0.012 for **1**, 0.048 ± 0.002 for **1a** and 0.521 ± 0.014 for **2** in 1,4-dioxane/dimethyl sulfoxide (v/v, 99/1) as well as for **1** 0.126 ± 0.003 in aqueous solution (ACN/water, v/v, 1/3). The triplet PS **2** generates more ¹O₂ than **1** and **1a** in ACN and exhibits very similar Φ_{Δ} values in both polar and non-polar solvents. The intersystem crossing (ISC) process in **2**, caused by the heavy atom effect of the two bromine atoms, results in a well populated triplet state (T_1), which is less dependent on the solvent polarity.^{25,32} and works more efficiently in polar solvents than in **1**. The PS **1** exhibits a

similar Φ_{Δ} value in non-polar environments to that of **2**, and shows a higher Φ_{Δ} value compared to its behaviour in more polar solvents. In contrast, **1a** displays the opposite trend: it has a higher Φ_{Δ} value in polar solvents and a lower Φ_{Δ} value in non-polar environments. In **1**, two deactivation pathways from the S_1 state to the T_1 state are conceivable. Firstly, ISC, which is typical for heavy atom containing triplet PS,^{13,16,28} and secondly, a spin-orbit charge-transfer (SOCT)-ISC process, which is predominates in heavy atom-free triplet PS,^{33,34,35,36} such as PET-based PS, where a charge-separated ¹CT state is formed and stabilized in polar solvents.³⁴ In general, the SOCT-ISC proceeds much faster than the ordinary ISC between π to π^* states.³⁷ For the heavy atom-free triplet PS **1a**, we observed a higher Φ_{Δ} value in polar solvents compared to the reference F-BODIPY **2a** ($\Phi_{\Delta} = 0.09$ in ACN)³⁸. This enhancement is likely due to a (SOCT)-ISC process facilitated by the polar environment. Moreover we observed similar Φ_{Δ} values for **1** and **1a** in ACN, indicating that in both PS, the SOCT-ISC is likely the predominant pathway from the ¹CT state to the T_1 state, in **1** the SOCT-ISC process likely predominates in polar solvents whereas conventional ISC is more dominant in non-polar environments.²⁵

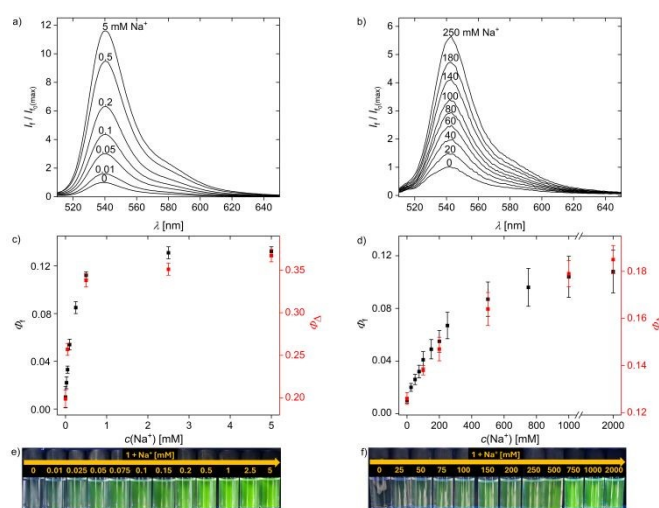


Figure 2 Fluorescence intensity (I_f) of **1** ($c = 10^{-6}$ M, $\lambda_{\text{ex}} = 500$ nm) in the presence of different Na⁺ concentrations a) in ACN and b) in ACN/water, (v/v, 1/3). Fluorescence quantum yields (Φ_f) (black) and singlet oxygen quantum yields (Φ_{Δ}) (red) of **1** in the presence of different Na⁺ concentrations c) in ACN and d) in ACN/water (v/v, 1/3). Photographs under UV light (366 nm) of **1** ($c = 10^{-6}$ M) in the presence of different Na⁺ concentrations e) in ACN and f) in ACN/water (v/v, 1/3).

Further, we recorded UV/Vis absorption spectra of **1** ($c = 10^{-5}$ M) in the presence of Na⁺ in ACN and in an ACN/water mixture of 1/3 (v/v) (cf. Figures S3a and S3b). The absorption at 540 nm (λ_{\max}) is nearly unaffected by Na⁺. The complexation of Na⁺ within the benzo-15-crown-5 in **1** can be observed by an enhanced blue-shift of the $\pi \rightarrow \pi^*$ transition from around 280 nm to 270 nm, (cf. Figures S3a and S3b) which is typical for cation complexation of benzo-crown ethers.³⁹ Then, we measured the influence of Na⁺ on the fluorescence intensity (I_f), Φ_f and Φ_{Δ} of **1** in ACN and aqueous solution (ACN/water, v/v, 1/3). The I_f of **1** is enhanced with increasing Na⁺ concentrations in ACN and aqueous solution (ACN/water, v/v, 1/3) (cf. Figures 2a and 2b). The relative course of both titration curves ($\lambda_{\text{em}} = 540$ nm, cf. Figures S7b and S7d) is similar but the maximum FE is reached at different Na⁺ concentrations, in ACN at 5 mM and in



aqueous solution (ACN/water, v/v, 1/3) at 2 M, respectively. The fluorescence enhancement factor (FEF) induced by Na⁺ in ACN is 11.6 ± 0.1 at 5 mM Na⁺ and in ACN/water (v/v, 1/3) is 9.1 ± 0.5 at 2 M Na⁺, respectively. We also observed an enhancement of the Φ_f values of **1** in the presence of different Na⁺ concentrations in ACN and aqueous solutions (ACN/water, v/v, 1/3) (cf. Figure 2c and 2d, Tables S4 and S5). Here, we observed the highest Φ_f value for **1** at 5 mM Na⁺ in ACN ($\Phi_f = 0.132 \pm 0.004$) and in aqueous solution (ACN/water, v/v, 1/3) at 2000 mM Na⁺ ($\Phi_f = 0.108 \pm 0.016$). Probably, the FE is caused by blocking the PET process in **1** by Na⁺, as also found for **1a** + Na⁺.²² Na⁺ raises the oxidation potential of the PET electron donor benzo-15-crown-5 in ACN and aqueous solution.⁴⁰ Therefore, the reductive PET process in **1** + Na⁺ becomes more unlikely as expressed by the Rehm-Weller equation.³⁰ Moreover, we also determined an enhanced Φ_A value for **1** in the presence of different Na⁺ concentrations in both ACN and aqueous solution (ACN/water, v/v, 1/3), (cf. Figure 2c and 2d, Tables S1 and S2). We also observed the highest Φ_A value for **1** at 5 mM Na⁺ in ACN ($\Phi_A = 0.367 \pm 0.007$) and in aqueous solution (ACN/water, v/v, 1/3) at 2000 mM Na⁺ ($\Phi_A = 0.185 \pm 0.006$). Moreover, we determined for **1a** + 5 mM Na⁺ a Φ_A value of 0.137 ± 0.006 in ACN which is close to the Φ_A value of 0.09 of **2a** in ACN³⁸. Overall, we observed for **1** an enhancement of I_f , Φ_f and Φ_A by Na⁺ and for **1a** an enhancement of I_f and Φ_f but a reduction of Φ_A by Na⁺ in polar solvents.

Further, we calculated the limit of detection (LOD) from the fluorescence titration data of **1** + Na⁺ (LOD = $3\sigma/m$) in ACN and aqueous solution (ACN/water, v/v, 1/3).²⁵ The PS **1** shows a lower sensitivity towards Na⁺ in ACN with a LOD of $(9.45 \pm 0.6) \mu\text{M}$ as in aqueous solution (ACN/water, v/v, 1/3) (11.5 ± 1.1 mM, respectively) (cf. Figures S9a and S9b). We also found a good linear relationship between the fluorescence intensity of **1** + Na⁺ in ACN and aqueous solution (ACN/water, v/v, 1/3) (from 0 mM to 0.14 mM Na⁺, $R^2 = 0.9966$ (ACN), from 0 mM to 100 mM Na⁺, $R^2 = 0.9992$ (ACN/water, v/v, 1/3), cf. Figures S9a and S9b) at 540 nm, respectively. More importantly, we calculated from the fluorescence intensity changes of **1** + Na⁺ their dissociation constants (K_d) in ACN and in aqueous solution (ACN/water, v/v, 1/3) resulting in K_d values of (0.16 ± 0.02) mM and (209 ± 5) mM, respectively.²⁵ The latter K_d value of **1** + Na⁺ in aqueous solution is biologically relevant, since it is close to the Na⁺ level in malign breast cancer cells.⁴ The K_d value of **1** + Na⁺ is significantly lower in ACN than in aqueous solution caused by the fact that a solvent like ACN that does not coordinate strongly with Na⁺ and a complexation of Na⁺ within the benzo-15-crown-5 is less hampered. In addition to it, the slopes of the plots for **1** + Na⁺ ($\log(c_{\text{Na}^+})$ vs $\log[(I_f - I_{f\text{min}})/(I_{f\text{max}} - I_f)]$) in ACN and aqueous solution (ACN/water, v/v, 1/3) were nearly 1 (cf. Figures S8a and S8b)²⁵, suggesting a 1:1 binding ratio between Na⁺ and **1**.

Moreover, to elucidate the binding stoichiometry between **1** with NaClO₄ in solution, we carried out ¹H NMR experiments in CD₃CN (cf. Figure S12).²⁵ Thus, a 1:1 binding stoichiometry of **1** with NaClO₄ was confirmed by a Job's plot analysis (cf. Figures S13).²⁵ We observed a downfield shift of the benzo-15-crown-5 protons until one equivalent NaClO₄ in the ¹H NMR spectra of **1** (cf. Figure S12) assuming that Na⁺ is coordinated within the benzo-15-crown-5 in **1**.

EPR experiments were carried out with 2,2,6,6-tetramethylpiperidine (TEMP) as a ¹O₂ specific spin-trap

agent.²⁵ It was added to **1** and **1** + 5 mM NaClO₄ and a strong EPR signal of 2,2,6,6-tetramethylpiperidinyloxy (TEMPO) was observed after light irradiation in ACN (cf. Figure S30). We found for **1** + 5 mM NaClO₄ a two times higher intensity of the TEMPO signal at 336.58 mT than for **1** indicating that in the presence of Na⁺ more ¹O₂ is produced.

We further investigated the influence of varying aqueous pH values on the fluorescence performance of **1**.²⁵ **1** shows very stable invariant fluorescence emission signals in the pH value range from 3.04 to 10.04 (cf. Figure S11a). Moreover, we observed for **1** in ACN and aqueous solution (ACN/water, v/v, 1/3) over a time period of 360 min a relatively photostable fluorescence signal at 540 nm (cf. Figure S11b) meaning that the photobleaching of **1** is negligible.

To verify selectivity of **1** for Na⁺ towards other important biological cations such as Li⁺, K⁺, NH₄⁺, Mg²⁺, Ca²⁺, Mn²⁺, Fe³⁺, Cu²⁺ and Zn²⁺, we measured the fluorescence intensities in the presence of these cations at their respective concentrations that are biologically relevant in aqueous solution (ACN/water, v/v, 1/3).²⁵ The fluorescence performance of **1** is only slightly impacted (cf. Figure S10), showing that **1** is a Na⁺-selective fluorescent imaging tool.

Moreover, we tested the DNA cleavage activity of **1** ($c = 200 \mu\text{M}$) with plasmid DNA at pH 7.4 with or without green light irradiation in the absence or presence of NaCl (cf. Figure 3) or NaClO₄ (cf. Figure S28). Degradation of supercoiled DNA (form I) to open-circular/nicked (form II) and linear DNA (form III) was monitored via gel electrophoresis.²⁵ Under green light irradiation, we observed DNA cleavage by **1** (lane j) forming 69% DNA form II (single-strand breaks) and even 1% form III (double-strand breaks). When the sample was not irradiated, no cleavage activity of **1** was observed (lane d about 40% form II). Surprisingly, the cleavage activity is not enhanced by NaCl (lanes k and l, Figure 3) or NaClO₄ (Figure S28). Probably, the stabilisation of the negatively charged DNA double helix (phosphate backbone) by Na⁺ due to electrostatic interactions⁴¹ results in a lower DNA cleavage activity of **1**.

Further, we crystallized **1** with NaClO₄ in a molar ratio of 1 : 1 from a chloroform/acetonitrile (v/v, 3/1) mixture to get more insights on the binding characteristics of Na⁺ within **1**. X-ray analysis provided the molecular structure of the Na⁺ complex [Na(**1**)(ClO₄)] (cf. Figure 4). Na⁺ is mainly coordinated by the five oxygen atoms of the benzo-15-crown-5 in **1** and shows a good fit-in-size into the cavity (cf. Figure 4a). Notably, the two symmetry-equivalent bridging perchlorate anions are disordered which influences the total number of coordination bonds of the Na⁺ (cf. Figures S23 and S24). We also found an electronical decoupling of the F-BODIPY from the Na⁺ complexed benzo-15-crown-5 unit because in the molecular structure of [Na(**1**)(ClO₄)] the phenyl ring is almost orthogonal to the planar F-BODIPY core (dihedral angle 82.2°, cf. Figure 4b).



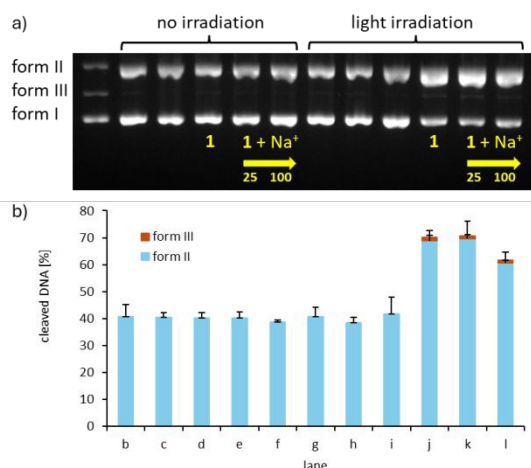


Figure 3 a) Nuclease activity towards plasmid DNA pBR322 (0.025 $\mu\text{g}/\mu\text{L}$) of PS **1** ($c = 200 \mu\text{M}$) in Tris buffer (5 mM, pH 7.4) w/o NaCl (25 or 100 mM). Samples in lanes g–l were incubated for 50 min under irradiation by green light for 50 min whereas samples in lanes a–f were not irradiated. Lane a: DNA ladder (form I, II and III), lane b + g: DNA reference, lanes c + i: 100 mM NaCl, lanes d + j: **1**, lanes e + k: **1** + 25 mM NaCl, lanes f + l: **1** + 100 mM NaCl, lane h: 25 mM NaCl. b) Visualization of the extent of DNA cleavage in percent with standard deviation as error bars.

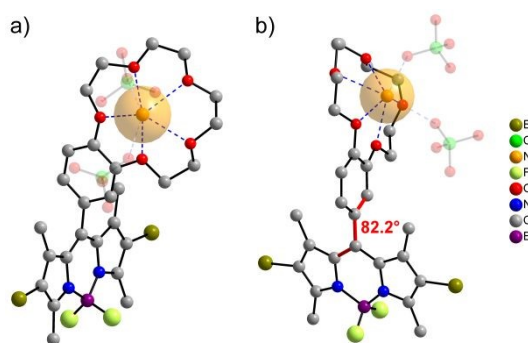


Figure 4 Molecular structure of $[\text{Na}(\mathbf{1})\text{ClO}_4]$ with a space-filling model of Na (crystal radius⁴² regarding coordination number). a) Front view and b) side view. H atoms are omitted for clarity.

Complementary to the experiments, we performed (time-dependent) density functional theory [(TD-)DFT] and singlet/triplet spin-orbit coupling (SOC) calculations of **1**, a dibromine-free F-BODIPY dye **1a** and **2** at the B3LYP/def2-TZVP level of theory^{43–45} in ORCA 6.0^{46,25}. The bright S_1 state of **1** in Figure 5c is given by a local transition on the BODIPY part from MO_{Dye} to the LUMO, while the optically dark ^1CT state shows strong charge transfer character from MO_{CT} to the LUMO. We find that the addition of Na^+ leads to an energetic stabilization of the MO_{CT} , while the two BODIPY-localized MOs remain mostly unaffected as shown in Figure 5d due to the greater spatial distance to the crown ether part of **1**. The excitation energy of the ^1CT state is thus increased relative to the bright S_1 state after Na^+ complexation in agreement with the reported experimental findings.²⁵ Furthermore, bromination leads to a one order of magnitude increase in the computed singlet/triplet SOC of **1** compared to **1a** due to the heavy-atom effect of the bromine atoms.²⁵

Overall, the fluorescence quenching observed for **1** is likely due to a reductive PET process. In polar solvents, a ^1CT state is formed

and stabilized, and its conversion to T_1 state via a SOCT-ISC mechanism is probable. The resulting T_1 state subsequently generates a moderate amount of $^1\text{O}_2$ in polar solvents. Furthermore, we assume that Na^+ interrupts the reductive PET process in **1** in polar solvents, leading to an increase in the energy of the ^1CT state. As a result, population of the T_1 state via ISC, facilitated by the heavy atoms (bromine), becomes more favourable and efficient, thereby restoring both fluorescence and $^1\text{O}_2$ generation of the dibrominated F-BODIPY core (cf. Φ_f and Φ_A values of **2** in polar media). As a result we observed for **1** + Na^+ higher Φ_f and Φ_A values compared to **1** without Na^+ (cf. Figures 5a and 5b). The latter can lead to degradation of DNA under irradiation (cf. Figures 3a and 3b). Moreover, we found for the dibromine-free F-BODIPY dye **1a** in the presence of Na^+ also an enhanced Φ_f value but a reduced Φ_A value in polar solvents. The presence of Na^+ blocks the reductive PET process in **1a**, resulting in an elevation of the ^1CT energy level. This effectively restores the fluorescence of the dibromine-free F-BODIPY core, where intersystem crossing (ISC) is considered highly unlikely (cf. Figures S34a and 34b). To the best of our knowledge, this is the first report that only a cation, here Na^+ , regulates $^1\text{O}_2$ evolution. The enhanced $^1\text{O}_2$ production by Na^+ can be useful to selectively kill malign cancer cells after irradiation when the K_d value of the Na^+ -selective PS fits to the Na^+ levels in the cancer cells.

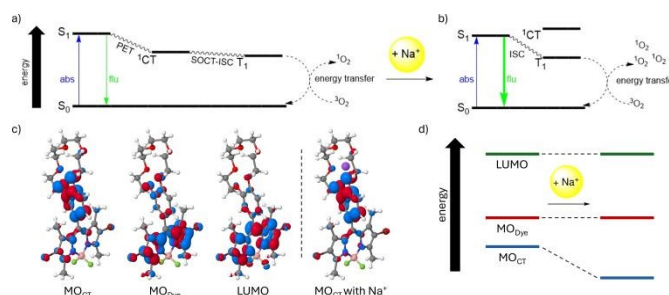


Figure 5 Jablonski diagram of the postulated mechanism of the photosensitized production of $^1\text{O}_2$ in the PS **1** in polar solvents a) without Na^+ and b) with Na^+ . c) Molecular orbitals (MOs) of **1** corresponding to the S_1 and ^1CT excited states (see further explanations in the text). d) Relative MO energy level changes of **1** due to the addition of Na^+ .

3 Conclusions

In summary, we synthesized the novel and Na^+ selective PS **1** consisting of a benzo-15-crown-5 and a dibrominated F-BODIPY dye shows a fluorescence signal which is photostable and invariant to a wide pH value range from 3.04 to 10.04. Further, **1** is a fluorescent tool with high Na^+ selectivity and Na^+ sensitivity, fast Na^+ response and the Na^+ induced fluorescence enhancement is even recognizable with the naked eye after irradiation with UV light. Moreover, we observed higher Φ_f and Φ_A values for **1** in the presence of Na^+ in polar solvents. The K_d value of **1** + Na^+ is (209 ± 5) mM in aqueous solution and fits better to the Na^+ level in malign cancer cells (around 100 mM Na^+) than to benign cells (around 20 mM Na^+).⁴ PS **1** is a suitable therapeutic as well as a Na^+ imaging agent. **1** could be a useful PS for cancer therapy because **1** could image tumorous tissue,



and targeted light irradiation would selectively kill cancer cells through $^1\text{O}_2$ generation. Currently, we are designing PSs applicable in PDT for a deeper tissue penetration by extending the π -system in position 2 and 5 of the F-BODIPY core to shift absorbance to the near-infrared (NIR) region.⁴⁷

Author contributions

Thomas Schwarze: conceptualization, methodology, investigation, formal analysis, writing – original draft; Mazen Al Akrami: investigation, data curation; Julian Heinrich: formal analysis, data curation; Vinja Hergl: investigation; Alexandra Kelling: formal analysis; Eric Sperlich: formal analysis, visualisation, methodology; Tobias Sprenger: formal analysis; Nicolas Jahn: formal analysis, visualisation; Tillmann Klamroth: supervision; Nora Kulak: funding acquisition, supervision, writing – review & editing.

Conflicts of interest

The authors declare no conflict of interest.

Data availability

The data supporting this article have been included as part of the ESI.†

Acknowledgements

The authors thank Matthias Hartlieb for providing access to a PhotoCube reactor (ThalesNano). The German Research Foundation (DFG) is acknowledged for funding within SFB 1636 (Project ID 510943930) for establishing EPR experiments under irradiation.

Notes and references

- Y. Allamyradov, J. ben Yosef, B. Annamuradov, M. Ateyeh, C. Street, H. Whipple and A. O. Er, *Photochem*, 2024, **4**, 434.
- J. F. Algorri, M. Ochoa, P. Roldán-Varona and J. M. López-Higuera, *Cancers*, 2021, **13**, 4447.
- A.-G. Niculescu and A. M. Grumezescu, *Appl. Sci.*, 2021, **11**, 3626.
- R. Ouwerkerk, M. A. Jacobs, K. J. Macura, A. C. Wolff, V. Stearns, S. D. Mezban, N. F. Khouri, D. A. Bluemke and P. A. Bottomley, *Breast Cancer Res. Treat.*, 2007, **106**, 151.
- L. O. Poku, M. Phil, Y. Cheng, K. Wang and X. Sun, *J. Magn. Reson. Imaging*, 2021, **53**, 995.
- J. M. Dubach, E. Lim, N. Zhang, K. P. Francis and H. Clark, *Integr. Biol.*, 2011, **3**, 142.
- O. Iamshanova, P. Mariot, V. Lehenkyi and N. Prevarskaya, *Eur. Biophys. J.*, 2016, **45**, 765.
- J. P. Celli, B. Q. Spring, I. Rizvi, C. L. Evans, K. S. Samkoe, S. Verma, B. W. Pogue and T. Hasan, *Chem. Rev.*, 2010, **110**, 2795.
- H. Luo and S. Gao, *J. Control. Release*, 2023, **362**, 425.
- A. Kamkaew, S. H. Lim, H. B. Lee, L. V. Kiew, L. Y. Chung and K. Burgess, *Chem. Soc. Rev.*, 2013, **42**, 77.
- Z. Mao, J. H. Kim, J. Lee, H. Xiong, F. Zhang and J. S. Kim, *Coord. Chem. Rev.*, 2023, **476**, 214908.
- E. Bassan, A. Gualandi, P. G. Cozzi and P. Ceroni, *Chem. Sci.*, 2021, **12**, 6607. DOI: 10.1039/D5CP03172A
- T. Yogo, Y. Urano, Y. Ishitsuka, F. Maniwa and T. Nagano, *J. Am. Chem. Soc.*, 2005, **127**, 12162.
- J. Piskorz, W. Porolnik, M. Kucinska, J. Długaszewska, M. Murias and J. Mielcarek, *ChemMedChem*, 2021, **16**, 399.
- P. Rybczynski, A. Smolarkiewicz-Wyczachowski, M. Ziegler-Borowska, D. Kedziera, J. Piskorz, S. Bocian and A. Kaczmarek-Kedziera, *Int. J. Mol. Sci.*, 2021, **22**, 6735.
- S. Atilgan, Z. Ekmekci, A. L. Dogan, D. Guc and E. U. Akkaya, *Chem. Commun.*, 2006, 4398.
- S. O. McDonnell, M. J. Hall, L. T. Allen, A. Byrne, W. M. Gallagher and D. F. O'Shea, *J. Am. Chem. Soc.*, 2005, **127**, 16360.
- S. Ozlem and E. U. Akkaya, *J. Am. Chem. Soc.*, 2009, **131**, 48.
- S. Callaghan and M. O. Senge, *Photochem. Photobiol. Sci.*, 2018, **17**, 1490.
- W. Wu, X. Shao, J. Zhao and M. Wu, *Adv. Sci.*, 2017, **4**, 1700113.
- N. Kwon, H. Weng, M. A. Rajora and Gang Zheng, *Angew. Chem. Int. Ed.*, 2025, **64**, e202423348.
- T. Sprenger, T. Schwarze, H. Müller, E. Sperlich, A. Kelling, H.-J. Holdt, J. Paul, V. Martos Riaño, M. Nazaré, *ChemPhotoChem*, 2023, **7**, e202200270.
- E. N. Nuraneeva, E. V. Antina, G. B. Guseva, M. B. Berezin and A. I. V'yugin, *Inorg. Chim. Acta*, 2018, **482**, 800.
- R. M. Izatt, R. E. Terry, D. P. Nelson, Y. Chan, D. J. Eatough, J. S. Bradshaw, L. D. Hansen and J. J. Christensen, *J. Am. Chem. Soc.*, 1976, **98**, 7626.
- For detailed experimental and theoretical data see Supporting Information.
- E. N. Nuraneeva, G. B. Guseva, E. V. Antina, O. A. Lodochnikova, D. R. Islamov and L. E. Nikitina, *Dyes Pigment.*, 2022, **201**, 110202.
- W. Hu, X.-F. Zhang, X. Lu, S. Lan, D. Tian, T. Li, L. Wang, S. Zhao, M. Feng, J. Zhang, *J. Lumin.*, 2018, **194**, 185.
- Y. P. Rey, D. G. Abradelo, N. Santschi, C. A. Strassert and R. Gilmour, *Eur. J. Org. Chem.*, 2017, **15**, 2170.
- For **1**, a reductive PET process from the benzo-15-crown-5 to the dibrominated F-BODIPY core has a negative ΔG_{PET} value of -0.03 eV according to the Rehm-Weller equation $\Delta G_{\text{PET}} = E_{\text{ox}} - E_{\text{red}} - \Delta E_{00} - \Delta G_{\text{ion-pair}}$.²⁷ The oxidation potential (E_{ox}) of benzo-15-crown-5 is 1.00 V and the reduction potential (E_{red}) of **2** is -1.20 V vs Ag/AgNO₃ as the reference electrode in ACN.²³ In ACN, the ΔE_{00} value of **2** (533 nm) is about 2.33 eV (transition energy between the vibrationally relaxed ground and excited state of the fluorophore).²³ The attractive energy, $\Delta G_{\text{ion-pair}}$ is assumed to be -0.1 V.²⁸
- D. Rehm and A. Weller, *Isr. J. Chem.*, 1970, **8**, 259.
- A. P. de Silva, H. Q. N. Gunaratne, J.-L. Habib-Jiwan, C. P. McCoy, T. E. Rice, J.-P. Soumilion, *Angew. Chem.*, 1995, **107**, 1889.
- W. Hu, R. Zhang, X.-F. Zhang, J. Liu, L. Luo, *Spectrochim Acta A Mol Biomol Spectrosc.*, 2022, **272**, 120965.
- X. Zhang, Z. Wang, Y. Hou, Y. Yan, J. Zhao and B. Dick, *J. Mater. Chem. C*, 2021, **9**, 11944.
- M. A. Filatov, *Org. Biomol. Chem.*, 2020, **18**, 10.
- P. P. Chebotaev, A. A. Buglak, A. Sheehan and M. A. Filatov, *Phys. Chem. Chem. Phys.*, 2024, **26**, 25131.
- A. A. Buglak, M. O. Senge, A. Charisiadis, A. Sheehan and M. A. Filatov, *Chem. Eur. J.*, 2021, **27**, 9934.
- J. T. Buck, A. M. Boudreau, A. DeCarmin, R. W. Wilson, J. Hampsey and T. Mani, *Chem.*, 2019, **5**, 138.
- M. A. Filatov, T. Mikulchyk, M. Hodee, M. Dvoracek, V. N. K. Mamillapalli, A. Sheehan, C. Newman, S. M. Borisov, D. Escudero and I. Naydenova, *J. Mater. Chem. C*, 2025, **13**, 6993.
- C. J. Pederson, *J. Am. Chem. Soc.*, 1967, **89**, 7017.



ARTICLE

Journal Name

- 40 S. Kenmoku, Y. Urano, K. Kanda, H. Kojima, K. Kikuchi and T. Nagano, *Tetrahedron*, 2004, **60**, 11067.
- 41 Z.-J. Tan, S.-J. Chen, *Biophys. J.*, 2006, **90**, 1175.
- 42 R. D. Shannon, *Acta Cryst.*, 1976, **A32**, 751.
- 43 A. D. Becke, *J. Chem. Phys.*, 1993, **98**, 5648-5652.
- 44 C. Lee, W. Yang and R. G. Parr, *Phys. Rev. B*, 1988, **37**, 785.
- 45 F. Weigend and R. Ahlrichs, *Phys. Chem. Chem. Phys.*, 2005, **7**, 3297-3305.
- 46 F. Neese, *WIREs Comput. Mol. Sci.*, 2022, **12**, e1606.
- 47 W. Porolnik, W. Szczolko, T. Koczorowski, M. Falkowski, E. Wieczorek-Szweda and J. Piskorz, *Spectrochim Acta A Mol Biomol Spectrosc.*, 2024, **314**, 124188.

View Article Online
DOI: 10.1039/D5CP03172A



- The data supporting this article have been included as part of the Supplementary Information.

